Chapter 4

An analytical model for viscous flow dynamics of steady state tropical cyclones

4.1 Introduction

Tropical cyclones, also known as hurricanes and typhoons, are powerful storms that form over warm ocean water in tropical regions (Stull (2015)). Those storms are characterized by strong winds, heavy rainfall, storm surges, and sometimes even tornadoes. They form when warm, moist air rises from the ocean's surface, creating an area of low pressure (Miller (1958); Kurihara and Tuleya (1974); Pandey and Maurya (2017); Yadav et al. (2024)). This low pressure creates an imbalance of pressure, leading to winds blowing

The contents of this chapter are published in **European Journal of Mechanics / B Fluids**, (1), **111**(2024) 72–80.

from all directions towards the low-pressure area. Such winds sometimes turn into storms. Ocean water at least $26.5^0\ C$ warm, atmospheric instability caused by steep temperature gradient, moisture in the mid-troposphere, small vertical wind shear and Coriolis force together cause a storm (Emanuel (2003), Gray (1979), Anthes (2016)). The general analysis of fluid motion indicates such a storm to be a combination of translation as well as rotation if the vorticity vector is non-zero. The presence of low pressure facilitates a rotation by creating cyclostrophic balance.

As air rises, it cools down and condenses, forming clouds and releasing heat energy. This energy powers the storm, causing it to spin and grow stronger. The spin is a consequence of combined Coriolis-induced rotation, winds converging toward a central low-pressure, and the conservation of angular momentum (Emanuel (2005)). The strength of a tropical cyclone is measured using the Saffir-Simpson hurricane wind scale, which categorizes storms based on their sustained wind speed (the highest wind speed averaged over a one-minute interval 10m above the surface). Storms classified as Category 1 have sustained winds of 74 to 95 mph, while those classified as Category 5 have winds of 157 mph or more. Tropical cyclones can cause widespread damage and loss of life, especially in coastal regions. They can also disrupt transportation, communication, and other critical infrastructure. Accurate forecasting and early warning systems have helped to reduce the impact of these storms, but they still remain a big threat to many communities around the world. Mathematical modelling can provide valuable insights into the behaviour and characteristics of tropical cyclones, including their formation, intensity, and track.

The basic physical model of a tropical cyclone consists of a rotating system of winds around a low-pressure centre, called an eye. The winds spiral inward around the eye, and as they approach the centre, they pick up moisture and heat from the warm ocean water, which fuels the storm's development. The physical geometry of a tropical cyclone

is complex and consists of several zones. These zones comprise Eye, Eye wall, Rain-band and Outflow (the detailed descriptions will take place in Section 2).

Cohen et al. (2019) examined the gradient non-balance at the top of hurricanes and how this phenomenon relates to the warm core structures within these storms. Gradient non-balance refers to deviations from the balance of forces, such as pressure gradient and centrifugal forces, found in the rotating winds of hurricanes. They analysed observational data to investigate how these imbalances at higher altitudes interact with and affect the warm core, a region of relatively high temperatures at the storm's centre. Montgomery et al. (2009) provided a model of tropical cyclone which includes some important physical phenomena such as precipitation and evaporative cooling. They focused more on the thermodynamic properties associated with tropical cyclones. Bloor and Ingham (1987) introduced a mathematical model for the inviscid motion of the conical cyclone which enabled to derive solutions in a compact and closed form. They validated the theoretical model by comparing its predictions to data from two diverse experimental studies. Yet many fundamental questions about cyclones remain unanswered. Outflow is the outward movement of air at the storm's top, which helps lower pressure at the centre and supports intensification by allowing warm, moist air to flow in at the surface. Investigation related to outflow started recently (Chavas et al. (2017); Emanuel and Rotunno (2011); Davies-Jones and Wood (2006)). Coriolis force is one of the most crucial factors to take into account when trying to solve a cyclone model (Montgomery et al. (2009); Willoughby (1979)). Emanuel (1986) gave a theory for air-sea interaction for tropical cyclones. He tried to explore the importance of ambient instability and air-sea latent heat transfer in both the development and maintenance of tropical cyclones. Researchers observed that at the upper level, such storms can deviate from gradient wind balance, which Cohen et al. (2019) termed "gradient wind non-balance", but are valid everywhere else in the hurricane vortex (Chavas et al. (2017); Willoughby (1979); Duran and Molinari (2018)). Bryan and Rotunno (2009)

also focused on more comprehensive models to include gradient wind non-balance and the maximum strength of a tropical storm. Vyas and Majdalani (2006) presented an inviscid solution which describes the cyclonic motion of a bidirectional vortex in a cylindrical chamber and constructed a solution from Euler's equation. An analytical model of tropical cyclones was provided by Kieu and Zhang (2009) to study rapid intensification based on rotational expansion and central pressure declines. They divided the entire domain into two regions: i) a region with fixed radius, known as the radius of maximum wind, that contains the maximum exponential wind growth, and ii) a region outside of the first region with no vertical component of velocity. They considered a simplified version of the primitive equations with a linear first-order frictional term. Ying and Chang (1970) simulated a tornado-like vortex close to the ground in a lab. They found that the pressure in the turbulent ground boundary layer is nearly constant vertically, with the exception of the region surrounding the vortex core. Li et al. (2019) re-examined eye-wall contraction in tropical cyclones using 3D and axi-symmetric simulations. They employed two different methods suggested by Kieu (2012) and Stern et al. (2015) to determine the radius of maximum wind through theoretical analysis and simulation. Tornadoes and tropical cyclones differ in scale and formation processes, but both of them are axi-symmetric vortices and possess similar rotational dynamics. Ben-Amots (2016) examined tornado dynamics, including rotation, thermodynamics, and condensation. The tornado's funnel reduces pressure, drawing in air and water vapour from the cloud above. Aouaouda et al. (2019) presented a mathematical model for tropical cyclone development. It's based on transforming the equations of non-viscous, non-heat-conductive gas (air) motion into wind trajectory equations within an axially symmetric cylindrical domain. Numerical solutions of these equations reveal that wind velocity increases as steam condenses and air warms. Lee and Wurman (2005) presented a physically consistent three-dimensional axis-symmetric tornado structure that was derived from mobile Doppler radar and the Ground-based velocity track display method. By assuming cyclostrophic wind balance within a tornado, they were able to calculate the

core pressure deficit in tornadoes. There are several analytical vortex models available in the literature for tornadoes, dust-devils and some atmospheric vortices (Burgers (1948); Sullivan (1959); Rott (1958); Davies-Jones and Wood (2006)).

This paper mathematically models tropical cyclones, which also includes the effects of viscous terms. In this study, our goal is to advance the current understanding of tropical cyclone dynamics by examining the influence of eye size on various aspects, including radial and azimuthal velocities as well as cyclone intensity (that is, a combination of velocity, central pressure and storm size). By incorporating viscosity into our mathematical models, we aim to demonstrate how different combinations of eye and eye-wall sizes affect cyclone intensification processes. Our findings give answers to these queries:

(1) How does the size of an eye relative to that of a cyclone affect key aspects such as the three components of velocity, viz. radial, axial and azimuthal velocities, and what are the implications on cyclone intensity?

(2) What is the influence of viscosity on tropical cyclones with varying eye sizes, and how does this influence cyclone behaviour and intensification processes?

(3) How do changes in pressure within the rain-band region of tropical cyclones correlate with cyclone intensity?

4.2 Mathematical formulation of Cyclonic Vortex

4.2.1 Geometry

The eye of a tropical cyclone is a circular, cylindrical region of lower pressure, often calm and with sometimes clear skies, located at the storm's centre. It is surrounded by the eye-wall, which is the most violent and destructive part of the cyclone. The eye-wall is a ring

of intense thunderstorms, where the strongest winds and heaviest rains occur. Surrounding the eye-wall are rain bands (also called spiral bands), which are bands of thunderstorms that spiral outward and produce rainfalls and gusty winds associated with a tropical cyclone. These rain bands contain areas of both updrafts and downdrafts, contributing to the variable, heavy rainfalls and gusty winds as they pass over different regions. The outflow of a tropical cyclone is the upper-level wind that moves away from the centre of the storm. It is important for the development and sustainability of the storm, as it allows for continuous intake of warm and moist air above the surface. Thus, a cyclone may be considered as an annular cylinder. The main part of the cloud structure of a mature cyclone may be idealized as an axi-symmetric vortex. The geometric figure below describes the vertical cross-section of a cyclone. (Fig. 4.1)

4.2.2 Mathematical Model of Tropical Cyclone

We consider a three-dimensional steady axi-symmetric atmospheric vortex in cylindrical coordinates $(\tilde{r}, \tilde{\theta}, \tilde{z})$, where $\tilde{r}, \tilde{\theta}, \tilde{z}$ are respectively radial, azimuthal and axial coordinates. For modelling vortices, we consider viscous and incompressible flow and also assume that the vortex is rotating symmetrically about the vertical axis $\tilde{r} = 0$. The dynamic system of equations governing the motion of incompressible viscous fluid is given by

$$\left(\tilde{u}\frac{\partial \tilde{u}}{\partial \tilde{r}} + \tilde{w}\frac{\partial \tilde{u}}{\partial \tilde{z}} - \frac{\tilde{v}^2}{\tilde{r}}\right) = -\frac{1}{\rho}\frac{\partial \tilde{p}}{\partial \tilde{r}} + \nu\left(\frac{\partial^2 \tilde{u}}{\partial \tilde{r}^2} + \frac{1}{\tilde{r}}\frac{\partial \tilde{u}}{\partial \tilde{r}} - \frac{\tilde{u}}{\tilde{r}^2} + \frac{\partial^2 \tilde{u}}{\partial \tilde{z}^2}\right), \tag{4.1}$$

$$\left(\tilde{u}\frac{\partial \tilde{v}}{\partial \tilde{r}} + \tilde{w}\frac{\partial \tilde{v}}{\partial \tilde{z}} + \frac{\tilde{u}\tilde{v}}{\tilde{r}}\right) = \nu\left(\frac{\partial^2 \tilde{v}}{\partial \tilde{r}^2} + \frac{1}{\tilde{r}}\frac{\partial \tilde{v}}{\partial \tilde{r}} - \frac{\tilde{v}}{\tilde{r}^2} + \frac{\partial^2 \tilde{v}}{\partial \tilde{z}^2}\right), \tag{4.2}$$

$$\left(\tilde{u}\frac{\partial \tilde{w}}{\partial \tilde{r}} + \tilde{w}\frac{\partial \tilde{w}}{\partial \tilde{z}}\right) = -\frac{1}{\rho}\frac{\partial \tilde{p}}{\partial \tilde{z}} + \tilde{F}_z + \nu\left(\frac{\partial^2 \tilde{w}}{\partial \tilde{r}^2} + \frac{1}{\tilde{r}}\frac{\partial \tilde{w}}{\partial \tilde{r}} + \frac{\partial^2 \tilde{w}}{\partial \tilde{z}^2}\right), \tag{4.3}$$

together with the continuity equation

$$\frac{1}{\tilde{r}}\frac{\partial(\tilde{r}\tilde{u})}{\partial\tilde{r}} + \frac{\partial\tilde{w}}{\partial\tilde{z}} = 0, \tag{4.4}$$

where $\tilde{u}$, $\tilde{v}$, $\tilde{w}$, ν stand respectively for the radial, azimuthal, axial components of velocity and the kinematic viscosity. Besides, $\tilde{p}$ is pressure and $\tilde{F}_z$ buoyancy.

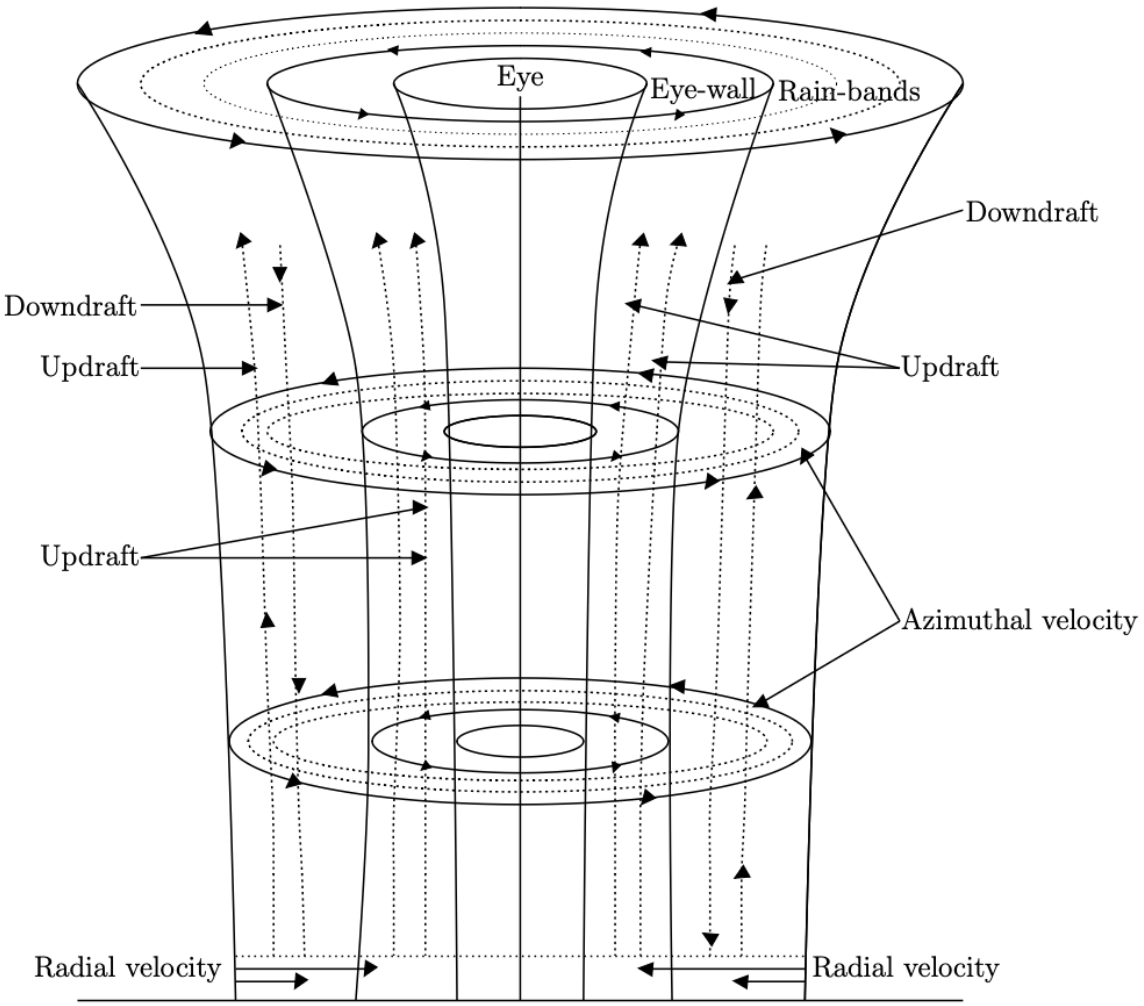

Figure 1: Schematic structure of tropical cyclone

Figure 4.1: Schematic structure of tropical cyclone

For the sake of dynamical similarity, we non dimensionalise the governing equations (4.1 - 4.4) by means of the following dimensionless variables

$$r = \frac{\tilde{r}}{r_m}, z = \frac{\tilde{z}}{r_m}, v = \frac{\tilde{v}}{v_m}, w = \frac{\tilde{w}}{v_m}, p = \frac{\tilde{p}}{\rho v_m^2}, F = \frac{\tilde{F}_z}{v_m^2/r_m};$$

v_m being the maximum azimuthal velocity at the radius r_m. Eq. (4.1 - 4.4) are transformed to

$$u\frac{\partial u}{\partial r} + w\frac{\partial u}{\partial z} - \frac{v^2}{r} = -\frac{\partial p}{\partial r} + \frac{1}{Re}\left(\frac{\partial^2 u}{\partial r^2} + \frac{1}{r}\frac{\partial u}{\partial r} + \frac{\partial^2 u}{\partial z^2} - \frac{u}{r^2}\right), \tag{4.5}$$

$$u\frac{\partial v}{\partial r} + w\frac{\partial v}{\partial z} + \frac{uv}{r} = \frac{1}{Re}\left(\frac{\partial^2 v}{\partial r^2} + \frac{1}{r}\frac{\partial v}{\partial r} + \frac{\partial^2 v}{\partial z^2} - \frac{v}{r^2}\right), \tag{4.6}$$

$$u\frac{\partial w}{\partial r} + w\frac{\partial w}{\partial z} = -\frac{\partial p}{\partial z} + F + \frac{1}{Re}\left(\frac{\partial^2 w}{\partial r^2} + \frac{1}{r}\frac{\partial w}{\partial r} + \frac{\partial^2 w}{\partial z^2}\right), \tag{4.7}$$

$$\frac{1}{r}\frac{\partial (ru)}{\partial r} + \frac{\partial w}{\partial z} = 0, \tag{4.8}$$

where, $Re = v_m r_m/\nu$ denotes the Reynolds number and $F = F_z/(v_m^2/r_m)$.

4.3 Empirical consideration of vertical wind

The vertical velocity of a tropical cyclone is an important parameter that helps to determine the strength and intensity of the storm. In order to construct a more comprehensive model, we consider vertical velocity dependent on radial and axial coordinates both.

There is a complex relationship between the radius and the vertical velocity of a tropical cyclone. In general, the vertical velocity of a tropical cyclone is maximum at the inner boundary of the eye-wall and declines radially outward from the inner boundary of the eye-wall. As the radius of the vortex increases with height, the vertical velocity of the cyclone seizes to zero. This is because as the vortex expands, the surface area, over which the cyclone dissipates its energy, also increases. This reduces the intensity of the

cyclone. Since the vertical velocity is maximum very close to the periphery of the eye and diminishes radially outward, it may be a function of sinusoidal form. So we may take vertical velocity in the following normalized form derived by Cecil and Majdalani (2022)

$$w = 2\eta kz\, cos[\eta(r^2 - \alpha^2)], \tag{4.9}$$

where α is the ratio of the radii of the eye and the cyclone respectively. $\eta = \frac{\pi}{1-\alpha^2}$ and $k = \frac{1}{2\pi\rho l}$, where the modified swirl number ρ i.e., the reciprocal of the normalized volumetric flow rate, l the aspect ratio which is the length of the swirl chamber normalized by its width, and inflow parameter k are taken from Vyas and Majdalani (2006). Since these parameters are related to laboratory experiment, the details can be seen in Vyas and Majdalani (2006), Cecil and Majdalani (2022). Substituting the axial velocity w into continuity Eq. (4.8), we obtain radial velocity as

$$u = -\frac{ksin[\eta(r^2 - \alpha^2)]}{r}. \tag{4.10}$$

Substituting $u(r, z)$ and $w(r, z)$ into $r-$ momentum Eq. (4.5), we get

$$\frac{v^2}{r} - \frac{\partial p}{\partial r} = -\frac{2\eta^2 k}{Re} sin[\eta(r^2 - \alpha^2)]. \tag{4.11}$$

Again substituting $u(r, z)$ and $w(r, z)$ into $z-$ momentum Eq. (4.7), we obtain

$$\frac{\partial p}{\partial z} = \frac{1}{Re}\Big(- 8\eta^2 kzsin[\eta(r^2 - \alpha^2)] - 8\eta^3 kr^2 zcos[\eta(r^2 - \alpha^2)]\Big) - 4\eta^2 k^2 z. \tag{4.12}$$

Integrating Eq. (4.12), with respect to z, we get

$$p = \frac{1}{Re}\Big(-4\eta^2 kz^2 sin[\eta(r^2-\alpha^2)] - 4\eta^3 kr^2 z^2 cos[\eta(r^2-\alpha^2)]\Big) - 2\eta^2 k^2 z^2 + f(r), \tag{4.13}$$

where $f(r)$ is a function of r appearing due to integration. Differentiating Eq. (4.13) with respect to r, we get

$$\frac{\partial p}{\partial r} = \frac{1}{Re}\Big(- 16\eta^3 z^2 krcos[\eta(r^2-\alpha^2)] + 8\eta^4 kz^2 r^3 sin[\eta(r^2-\alpha^2)]\Big) + f'(r). \quad (4.14)$$

4.4 Evaluation of *f(r)*

To evaluate the arbitrary function $f(r)$, we use Vatistas et al. (1991) model as a boundary condition at $z = 0$. The model involves the azimuthal component of velocity v for incompressible and steady flow given by.

$$v = \frac{r}{(r^{2n}+1)^{1/n}}, \quad (4.15)$$

in dimensionless form, where r is the radial coordinate normalized by r_m and n dictates how tangential velocity v changes with radial distance r from the vortex centre is called power-law index. We further take a particular case of Vatistas's velocity for $n = 2$ as the velocity profile for $n = 2$ is most practical and quite similar to the velocity profiles obtained by the previous models such as Rankine and Burgers models. An additional assumption is that the flow is in the cyclostrophic balance at $z = 0$, i.e.

$$\frac{v^2(r,0)}{r} = \frac{\partial p(r,0)}{\partial r}, \quad (4.16)$$

$$\frac{r}{(r^4+1)} = \frac{\partial p}{\partial r}. \quad (4.17)$$

Substituting $z = 0$ in Eq. (4.13), we get

$$f(r) = \int \frac{r}{r^4+1} dr, \quad (4.18)$$

$$f(r) = \frac{1}{2} tan^{-1} r^2, \tag{4.19}$$

$$p = \frac{1}{Re}\Big(- 4\eta^2 k z^2 sin[\eta(r^2-\alpha^2)] - 4\eta^3 k r^2 z^2 cos[\eta(r^2-\alpha^2)]\Big) - 2\eta^2 k^2 z^2 + \frac{1}{2} tan^{-1} r^2. \tag{4.20}$$

Substituting the above values into the $u-$momentum equation, we obtain

$$v^2 = k^2\left(\frac{2\eta r^2 cos[\eta(r^2-\alpha^2)] sin[\eta(r^2-\alpha^2)] - sin[\eta(r^2-\alpha^2)]}{r^2}\right) + \frac{1}{Re}\Big(- 16\eta r^2 cos[\eta(r^2-\alpha^2)] + 4\eta^2 r^2 z k(2\eta^2 z^2 r^2 - 1) sin[\eta(r^2-\alpha^2)]\Big) + \frac{r}{(r^4+1)}, \tag{4.21}$$

$$v = k\left[\left(\frac{2\eta r^2 cos[\eta(r^2-\alpha^2)] sin[\eta(r^2-\alpha^2)] - sin[\eta(r^2-\alpha^2)]}{r^2}\right) + \frac{1}{Re}\Big(- 16\eta r^2 cos[\eta(r^2-\alpha^2)] + 4\eta^2 r^2 z k(2\eta^2 z^2 r^2 - 1) sin[\eta(r^2-\alpha^2)]\Big) + \frac{r}{(r^4+1)}\right]^{1/2}, \tag{4.22}$$

4.5 Results and discussion

4.5.1 Axial velocity

The axial component of velocity is based on the assumption that it is a function of r and z, both for viscous, incompressible and steady flow. Fig. (4.2) depicts the radial profile of the axial velocity for different α. We plot normalized axial velocity given by Eq. (4.9) for $\alpha = 0 - 0.75$ versus r. For $\alpha = 0$, the radius of the eye is zero, which is not a real case because the eye is a region of a low-pressure area, without which cyclones cannot survive. However, we continue with it for the sake of comparison. Plots in Fig. (4.2) reveal that the axial velocity is minimum at $r = \sqrt{\frac{1+\alpha^2}{2}}$ (this may be deduced from Eq.

(4.9) by substituting the expression of η) which shifts away from the centre as α increases, and eventually for $\alpha = 1$, r will be 1 (for the sake of analysis, but definitely not a practical case). On the other hand, it reaches the maximum at the inner surface of the eye-wall for every α. It is further noticed that the higher the value of α, the greater the velocity at the interface of the eye and eye-wall. The growth in velocity is not linear with r. It is further observed that the gradient of the velocity decreases as we move toward the interface of the eye and the eye-wall. This may be interpreted physically as that the larger the eye size, the faster the updraft (outlined in Fig. (4.2)).

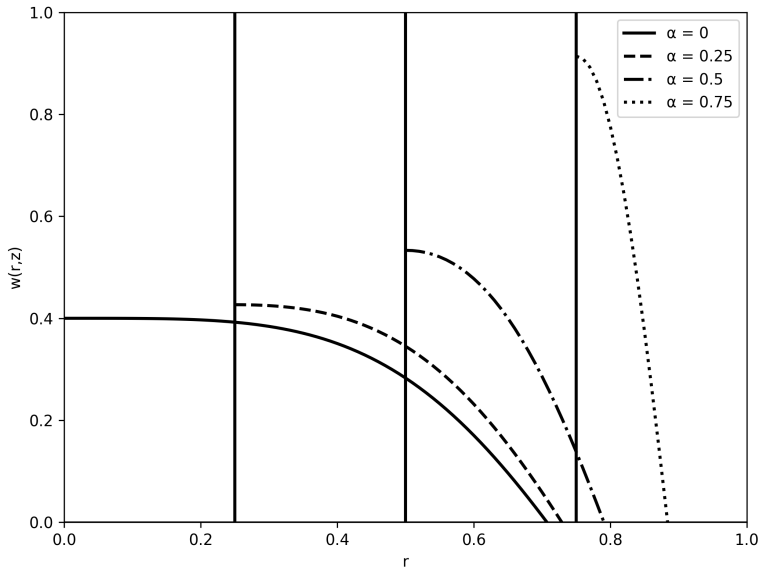

Figure 4.2: The plot presents the radial profiles of normalized axial velocities for $\alpha = 0, 0.25, 0.50, 0.75$ at $z = 0.5$, $k = 1$. The radial profiles are shown in the eye-wall but not the eye which is calm with no updraft.

For all the values of $\alpha = 0.25 - 0.75$, axial velocity increases near the eye region, and the maximum velocity is attained at the inner boundary of the eye-wall. Thus, we may conclude that in a cyclone, the updraft is concentrated close to the eye. If eye size is larger compared to the thickness of the eye-wall, the updraft has the tendency to rise faster.

4.5.2 Radial velocity

Fig. (4.3) displays the radial profile of radial velocity $u(r)$ for different α based on Eq. (4.10). It is observed that the radial velocity at the inner and outer interfaces of the eye-wall is zero but increases in magnitude in the middle of the eye-wall region. For $\alpha = 0$, there is a huge rise in the radial velocity in the middle of eye-wall.

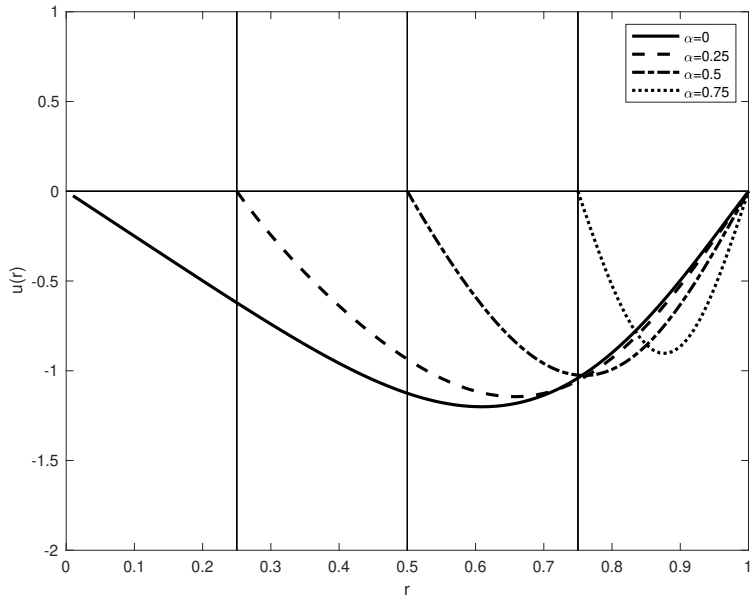

Figure 4.3: Normalized radial velocities for $\alpha = 0, 0.25, 0.50, 0.75$ at $z = 0.5$, $k = 1$. The negative values of u simply indicate that the radial velocity is directed towards the axis. The right hand side of the vertical lines indicate the beginning of corresponding eye-wall regions.

As α increases, which refers to a wider size of the eye and correspondingly a thinner eye-wall, the maximum radial velocity is found to decrease in the middle of eye-wall. The results are interpreted as that the greater the radial velocity, the thicker the eye-wall.

4.5.3 Azimuthal velocity

The azimuthal velocity is the most vital factor in the formation and survival of tropical cyclones. Higher azimuthal velocities generally lead to stronger and more intense storms, while lower azimuthal velocities are not adequate for their survival and let them dissipate quickly. When the eye-size is much smaller than that of the whole cyclone, the pattern of the azimuthal velocity follows the characteristics (outlined in Figs. 4.5-4.7).

As one moves radially outward, the azimuthal velocity increases rapidly. It reaches its maximum in the eye-wall. This is often the region where the most intense winds in the cyclone are found. Beyond the eye-wall, the azimuthal velocity exhibits a sinusoidal pattern. This means that the velocity fluctuates radially outward. These variations in velocity are typically associated with the rain bands of the cyclone. Moving away from the eye-wall and into the rain bands, the amplitude decreases. This implies that while there are still fluctuations in velocity, they are less prominent than those in the eye-wall. Eventually, as one moves radially outward even further into regions not strongly influenced by the cyclone's circulation, the azimuthal velocity decreases significantly and becomes negligible. This is often observed in the outer regions of the cyclone. Refan et al. (2017) gave a velocity profile analysis using the ground-based velocity track display method on Doppler radar data on tornadoes. They simulated the collected data for different heights against Rankine and modified Rankine models. However, the radial profiles of the azimuthal velocity given by Refan et al. (2017) are in good agreement with those of this model. As α increases, which refers to a wider size of eye and corresponding thinner eye-wall, the maximum azimuthal velocity is higher than that with a smaller eye. After reaching its peak intensity, the azimuthal velocity experiences a sudden fall. This fall is typically associated with the transition from the eye-wall to the outer regions of the cyclone.

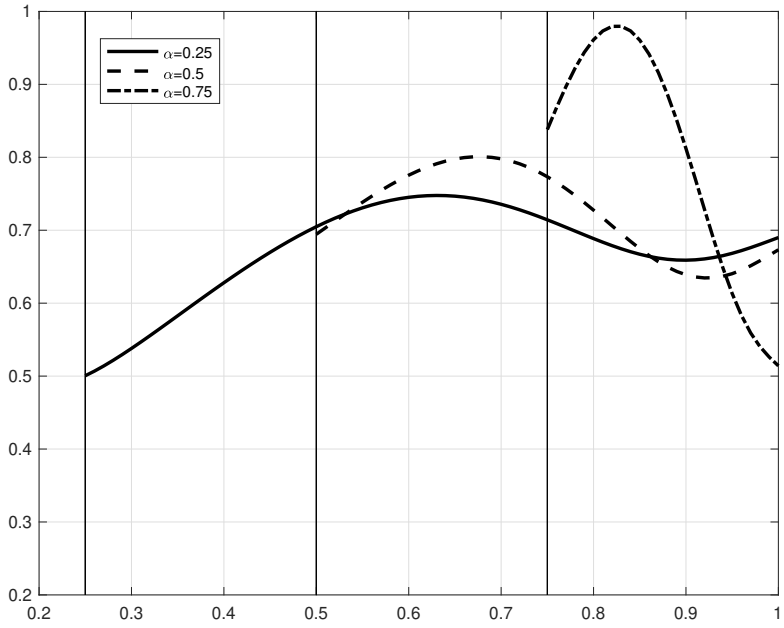

Figure 4.4: Normalized azimuthal velocities for $\alpha = 0, 0.25, 0.50, 0.75$ along r for $z = 0.5$ and $k = 1$. The right hand sides of the vertical lines indicate the beginning of the corresponding eye-wall regions followed by rain band regions (the interfaces of the two have not been indicated in the graph).

Smith (2006) provided a categorization of observations based on eye size, dividing them into small, medium, large, and those without an eye. This classification revealed associations between intensity and strength, which were not apparent when considering the entire sample. These correlations may become evident because eye size acts as a proxy for a phase of the cyclone's life cycle. The behaviour of azimuthal velocity in a tropical cyclone is influenced by the size of the eye relative to the cyclone's overall size. A smaller eye leads to intense winds in the inner eye-wall and a gradual decrease in intensity radially outward into the rain bands, while a larger eye results in even higher maximum wind intensity in the inner eye-wall but an abrupt fall in intensity beyond it, followed by the sinusoidal pattern in the rain bands.

In order to analyse the impact of Reynolds number on the cyclonic azimuthal velocity, we take Reynolds number in the range $1000 - 100000$ (Fig. 4.5-4.7). The azimuthal velocity curves corresponding to different Reynolds numbers are more distinct with increasing α, that is, when eye size increases with respect to the cyclone width. In the inner region of the eye-wall, cyclonic azimuthal velocity increases with Reynolds numbers, but as one moves radially outward, to some extent, the trends reverse. The difference in azimuthal velocities corresponding to different Reynolds numbers is at the maximum in the eye-wall, from where the differences start diminishing and continue so in the rainbands. At the point of the maximum difference, the azimuthal velocities for comparatively very high Reynolds numbers show a local minimum.

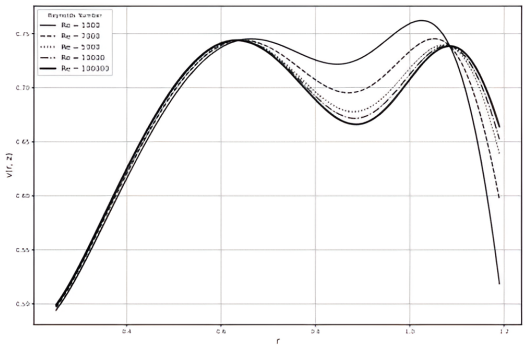

(a) Plot for $z = 0.8$

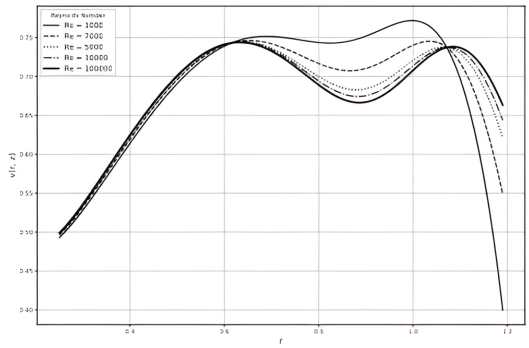

(b) Plot for $z = 1.0$

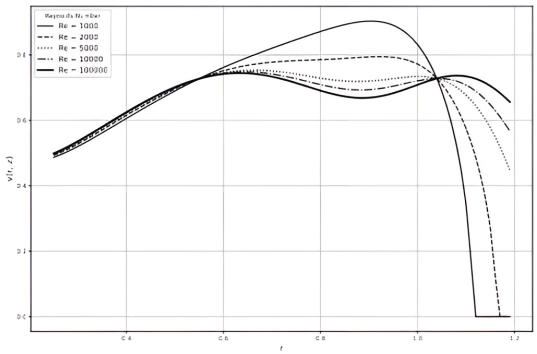

(c) Plot for $z = 2.0$

Figure 4.5: Plots for radial profiles of vertical velocity for $\alpha = 0.25$ and different heights ($z = 0.8$, $z = 1.0$, and $z = 2.0$).

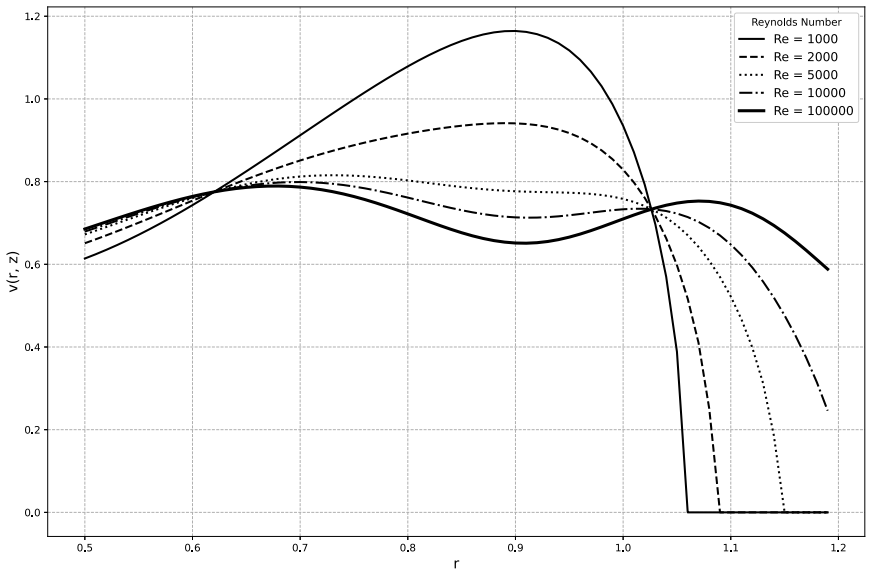

Figure 4.6: Normalized azimuthal velocities at $\alpha = 0.50$ for different Reynolds numbers Re for $z = 0.5$ and $k = 1$.

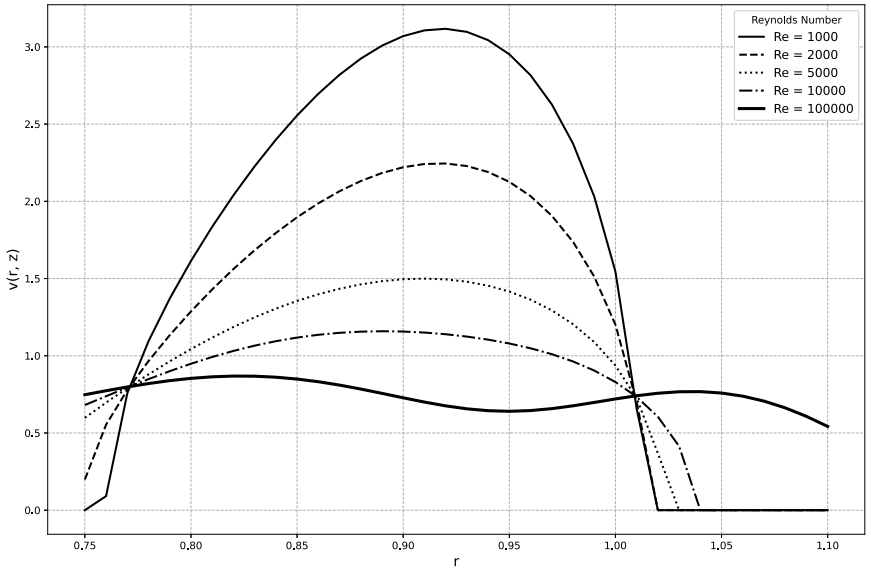

Figure 4.7: Normalized azimuthal velocities at $\alpha = 0.75$ for different Reynolds numbers Re and $z = 0.5$, $k = 1$.

Fig. (4.5)-(4.7) are plotted to display the impact of Reynolds number on azimuthal velocity for α ranging from $0.25 - 0.75$. The parts (a)-(c) of Fig. (4.5) demonstrate

the role played by z. In the inner eye-wall, we observe that at a particular radial length, say r_c, of course, depending on α, i.e., $\alpha < r_c < 1$, the Reynolds number does not play any significant role. In other words, all velocity curves merge at that point. In the inner region of eye-wall within r_c, azimuthal velocity increases slightly with Reynolds number. Beyond r_c the trend reverses i.e., azimuthal velocity decreases when the Reynolds number increases. In this region, the differences are higher. In addition, the velocity rises in this zone to a maximum depending on the Reynolds number. It is also observed that increasing the Reynolds number, the maximum velocity is comparatively less and is attained at a smaller radius for higher Reynolds numbers. The velocity curves once again merge for larger radial length i.e., in the rain-band. The velocities corresponding to all Reynolds numbers diminish further with the radial length to die out eventually. In Fig. (4.5)(a-c), we observe that the maximum azimuthal velocity slightly increases with altitude z for lower Reynolds numbers.

4.5.4 Pressure distribution

A major role in the development and survival of tropical cyclones is played by radial pressure. Figs. (4.8) and (4.9) show that pressure decreases from the outer region of the eye-wall to the axis of the vortex. The axial pressure gradient is derived by substituting the axial velocity and the derived radial velocity from the continuity equation into the z-momentum equation. Integration of the resulting equation gives pressure. To evaluate the undetermined function of integration $f(r)$, we use the Vatistas model as a boundary condition at $z = 0$. We assume the flow to be in the cyclostrophic balance i.e. $\frac{v^2(r,0)}{r} = \frac{\partial p(r,0)}{\partial r}$. We observe the variation of the size of a cyclone's core or eye and the pressure distribution within the cyclone, which provides valuable insights into the dynamics of tropical cyclones. Regardless of the specific values chosen for α, a consistent pattern emerges in cyclones with relatively small eyes compared to their overall size: the pressure

tends to increase radially outward (Outlined in Fig. (4.8)). This finding underscores the critical role played by the core of the cyclone, typically encompassing the calm and clear region known as the eye, in exerting lower pressure compared to the outer regions of the cyclone. Furthermore, our research reveals a significant correlation between the size of the eye and the overall intensity of tropical cyclones. Specifically, when a cyclone possesses a larger eye, the pressure within the cyclone is notably less compared to that with smaller eyes. This observation highlights the substantial influence of the eye size on a cyclone's intensity. Larger eyes characterize powerful storms.

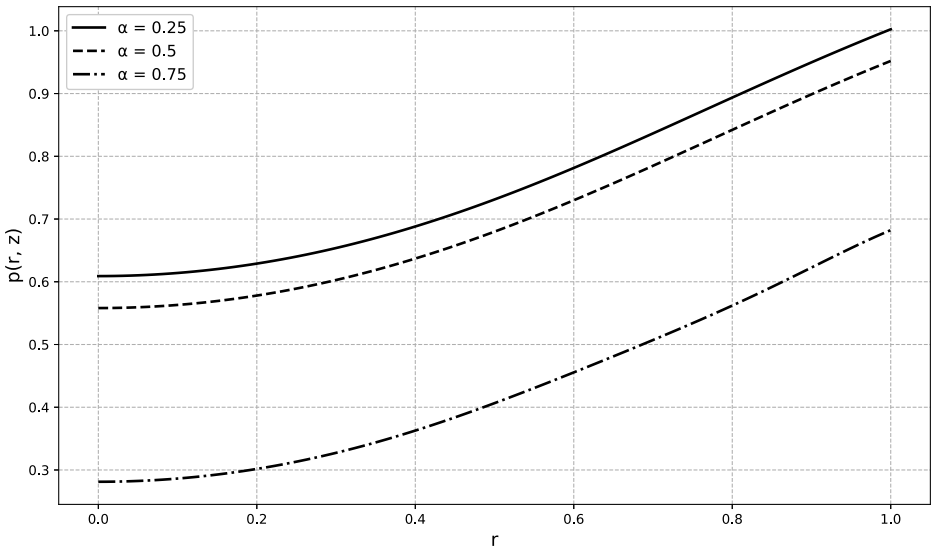

Figure 4.8: Radial profiles of pressure for $\alpha = 0.25, 0.5, 0.75$, $Re = 10000$, $z = 0.5$, $k = 1$.

In Fig. (4.9), z has been varied in the range $0.1 - 0.8$. The radial pressure distribution remains similar at all altitudes but pressure lower with increasing z.

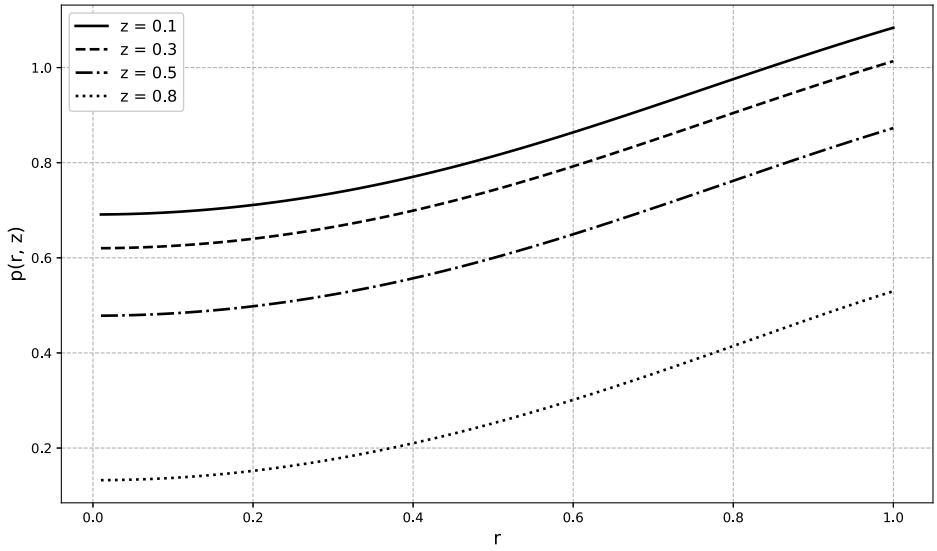

Figure 4.9: Radial profiles of pressure for different heights for $Re = 10000$, $k = 1$.

4.5.5 Radial Pressure Gradient

At the very centre of the cyclone, which is known as the eye, we will find the lowest pressure within the entire cyclone. This low-pressure centre is a defining feature of cyclones and contrasts sharply with the higher pressure outside the eye. As we move radially outward from the eye towards the outer regions of the cyclone, the radial pressure gradient gradually increases. Fig. (4.10) shows a fascinating pattern associated with cyclones with a relatively smaller eye ($\alpha = 0.25$). Pressure gradient consistently increases radially outward from the eye. However, as we continue moving away from the eye-wall into the rain band region, the pressure gradient gradually decreases.

In contrast, a rapid increase in pressure gradient behaviour is observed towards the eye-wall when tropical cyclones possess a larger eye, represented by $\alpha = 0.75$. This steep rise in pressure gradient highlights the significant influence exerted by larger eyes on the cyclone's intensity. However, towards the outer regions of the cyclone, there is a corresponding rapid drop in the pressure gradient. This suggests that in cyclones with

larger eyes, the pressure gradient diminishes more rapidly along the eye-wall into the rain band region, where the cyclone's impact lessens. This observation underscores the critical role played by the size of the eye in shaping the pressure gradient dynamics within cyclones and its implications for storm intensity.

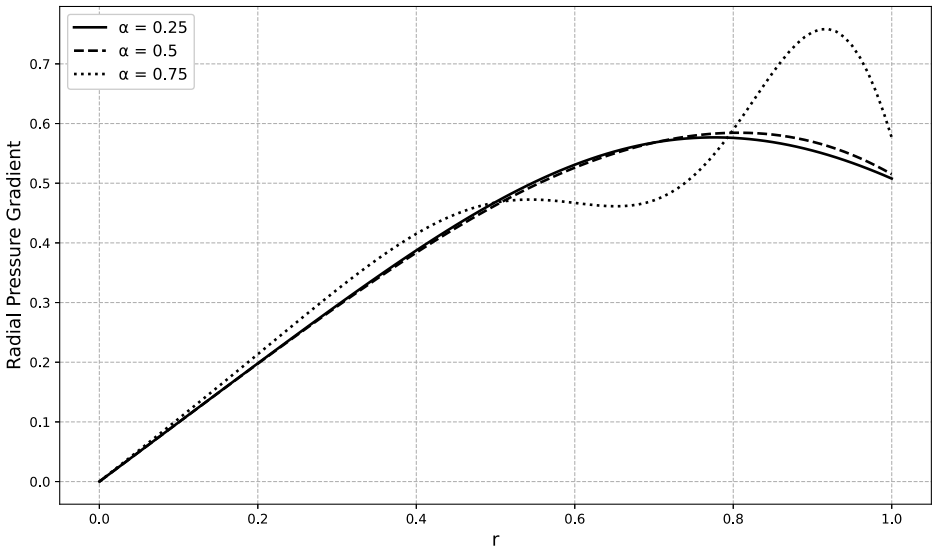

Figure 4.10: Radial profiles of pressure gradient for different α, $Re = 10000$, $k = 1$

4.6 Conclusion

The impact of eye size and viscosity on the motion of tropical cyclones and intensification are prominent concern. Unlike the formulations of Cecil and Majdalani (2022), the azimuthal velocity and pressure involve viscous terms in the present investigation.

Radial velocity, which is directed towards the vortex axis, is zero at the inner and outer interfaces of the eye-wall but gets magnified to a maximum in the mid-eyewall region. Also, larger radial velocity leads to thicker eye-wall.

Axial velocity (i.e., vertically upward wind motion), which increases linearly with the axial coordinate (z), is found to be maximum at the periphery of the eye, but

diminishes beyond that as one moves outward through the eye-wall. In a cyclone, the updraft is concentrated close to the eye. If eye size is larger compared to the thickness of the eye-wall, the updraft has the tendency to rise faster.

Azimuthal velocity increases slightly with higher Reynolds numbers in the inner eye-wall surrounding the eye. This pattern persists within the inner eye-wall, but reverses in the outer eye-wall enormously. It reaches a maximum in the outer eye-wall, beyond which the difference starts to decrease, rather slowly, and continues to do so within the rain bands. Thus, it is inferred that in the vicinity of the entire circumference of the maximum azimuthal velocity, the storms will be quite intense for viscous flow.

The size of the eye impacts the tropical cyclone quite significantly, with large eye-size relative to the cyclone width, comprises a severe storm in the eye-wall for high viscosity, which loses its intensity rapidly in the rain band region. This may be inferred that wind strength will be found to be less if the wind is considered inviscid.

Pressure increases radially outward irrespective of the eye-size, but diminishes in magnitude with eye-size as well as increasing altitude. Pressure gradient declines faster through the eye-wall into the rain band region for cyclones with larger eyes.

Even though this model takes care of the viscosity of the fluid and discusses the role of eye size or, equivalently eye-wall and rain-band width, the model is meant for steady motion, ignoring a rather more important aspect of the formation/genesis of cyclone, which could be possible only when non-steady equations are solved.

****